

Dark energy with oscillatory tracking potential: Observational Constraints and Perturbative effects

Albin Joseph^{*} and Rajib Saha[†]

¹*Department of Physics, Indian Institute of Science Education and Research (IISER) Bhopal, 462066, India*

Accepted XXX. Received YYY; in original form ZZZ

ABSTRACT

The cosmological models exhibiting tracker properties have great significance in the context of dark energy as they can reach the present value of dark energy density from a wide range of initial conditions, thereby alleviating both the fine-tuning and the cosmic coincidence problem. The α -attractors, which are originally discussed in the context of inflation, can exhibit the properties of dark energy as they can behave like cosmological trackers at early times and show the late time behaviour of a cosmological constant. In the present paper, we study the Oscillatory Tracker Model (OTM), which belongs to the family of α -attractor dark energy models. Using the current observational data sets like Cosmic Microwave Background (CMB), Baryon Acoustic Oscillation (BAO) and type 1a supernova data (Pantheon compilation), we constrain the parameters of the model and estimate both the mean and best-fit values. Although the oscillatory tracker model contains a larger set of parameters than the usual Λ CDM model, the common set of parameters of both agree within 1σ error limits. Our observations using both high redshift and low redshift data supports Hubble parameter value $H_0 = 67.4 \text{ Kms}^{-1}\text{Mpc}^{-1}$. We study the effect of the OTM on the CMB temperature and polarization power spectra, matter power spectrum and $f\sigma_8$. Our analysis of the CMB power spectrum and matter power spectrum suggests that the oscillatory tracker dark energy model has noticeable differences from usual Λ CDM predictions. Yet, in most cases, the agreement is very close.

Key words: dark energy – scalar fields – observational constraints

1 INTRODUCTION

The accelerated expansion of the universe, which was first discovered through the observations of type 1a supernovae (Riess et al. 1998; Perlmutter et al. 1999) serves as a paradigm shift in our understanding of cosmology. This hypothesis was strongly supported by the data from other observations like CMB anisotropies (Aghanim et al. 2020) or the large scale structure (Eisenstein et al. 2005; Blake et al. 2012; Parkinson et al. 2012; Kazin et al. 2014; Beutler et al. 2015). The current accelerated expansion is attributed to the so-called 'dark energy', and it provides a dominant contribution to the present total energy density of the universe. The contribution of the matter content of the universe is represented by the energy-momentum tensor on the right-hand side of the Einstein equation, whereas the left-hand side is represented by pure geometry. The accelerated expansion of the universe can be obtained either by supplementing the energy-momentum tensor by an exotic form of matter such as cosmological constant or scalar field and also by modifying the geometry itself.

Presently the most accepted cosmological model is the

Λ CDM model, which consists of a cosmological constant Λ , cold dark matter, baryons, photons and neutrinos. Though it can explain many observed cosmological phenomena, it has several theoretical inconsistencies like the fine-tuning (Sahni 2002) and the cosmic coincidence problems (Steinhardt 2003; Velten et al. 2014). This motivates cosmologists to look forward to alternate models for the explanation of cosmological dilemmas. So instead of considering a cosmological constant, dark energy is introduced as a dynamical phenomenon. Among them, the models such as Quintessence (Linder 2007; Tsujikawa 2013; Chiba et al. 2013; Durrive et al. 2018), Phantoms (Caldwell 2002; Caldwell et al. 2003; Nojiri et al. 2005; Ludwick 2018), K-essence (Chiba et al. 2000; Armendariz-Picon et al. 2000, 2001), Tachyon (Padmanabhan 2002; Bagla et al. 2003; Abramo & Finelli 2003; Aguirregabiria & Lazkoz 2004; Guo & Zhang 2004; Copeland et al. 2005) and Dilatonic Dark Energy (Piazza & Tsujikawa 2004; Damour et al. 2002) consider a scalar field as responsible for the dynamics of the dark energy. In an alternative approach, the accelerated expansion of the universe can be obtained from the geometrical modifications which can arise from quantum effects such as higher curvature corrections to the Einstein Hilbert action (Lobo 2008; Tsujikawa 2011; Li et al. 2011; Clifton et al. 2012; Dimitrijevic et al. 2013; Brax & Davis 2015; Joyce et al. 2016).

^{*} E-mail: albinje@iiserb.ac.in

[†] E-mail: rajib@iiserb.ac.in

As discussed above, the dark energy models are very successful in explaining the current accelerated expansion of the universe. On the other hand, the primordial inflationary models (Guth 1981) play a significant role in explaining other observed phenomena like the origin of CMB anisotropies (Abazajian et al. 2015) and the formation of the large scale structure (L’Huillier et al. 2018). The origin of early and late inflation still remains a theoretical puzzle that motivates the theorists to simultaneously explain both inflationary phases by invoking scalar fields. The scalar fields play a fundamental role in cosmology as they are simple, yet a natural candidate for the accelerated expansion of the universe. Presently there are wide variety of inflationary models (Guth 1981; Linde 1982, 1983) that have been proposed, and among them, the cosmological attractor models were discovered recently (Kallosh & Linde 2013). These cosmological attractor models belong to a wide class of cosmological models which incorporate the conformal attractors (Kallosh & Linde 2013), alpha attractors (Kaiser & Sfakianakis 2014; Kallosh et al. 2013, 2014; Miranda et al. 2017; Shahalam et al. 2018), and also include scalar field cosmological models such as the Starobinsky model (Starobinsky 1980; Mukhanov & Chibisov 1981; Starobinsky 1983; Whitt 1984; Kofman et al. 1985), the chaotic inflation in supergravity (GL model) (Goncharov & Linde 1984a,b; Linde 2015), the Higgs inflation (Salopek et al. 1989; Bezrukov & Shaposhnikov 2008; Cervantes-Cota & Dehnen 1995; Ferrara et al. 2010; Linde et al. 2011) and the axion monodromy inflation (Silverstein & Westphal 2008; McAllister et al. 2010; Conlon 2012; Flauger et al. 2010; Brown et al. 2016). The conformal attractor models predicts that for a large number of e-folds N , the spectral index and tensor-to-scalar ratio are given by $n_s = 1 - 2/N$; $r = 12/N^2$ whereas for alpha attractors, the slow-roll parameters are given by $n_s = 1 - 2/N$; $r = 12\alpha/N^2$ for small α and $n_s = 1 - 2/N$; $r = 12\alpha/(N(N + 3\alpha/2))$ for large α . Although these models have different origins, they provide very similar cosmological predictions with WMAP (Hinshaw et al. 2013) and the recently released Planck data (Aghanim et al. 2020). These models can be used not only for inflation but also for late-time cosmic acceleration. In the context of dark energy, the cosmological models with tracker properties have gained great attention as the scalar field can reach the present value of dark energy density from a wide range of initial conditions. Thus a scalar field rolling down a slowly varying potential not only gives rise to the current accelerated expansion but also alleviates the cosmic coincidence problem.

In the present work, we focus on a specific α -attractor dark energy model - the Oscillatory Tracker Model (OTM), which was initially proposed in (Bag et al. 2018). The OTM, with its tracker properties, can alleviate the cosmic coincidence problem and moreover, it is very much favoured over various other α -attractor dark energy models (Cedeño et al. 2019). Here we focus on testing the OTM against different cosmological observations like type 1a supernovae, BAO, and CMB. We also study the effect of the OTM on the CMB temperature and polarization power spectra, matter power spectrum and $f\sigma_8$ with respect to the background Λ CDM model.

This paper is structured as follows. In section 2, we present the basics of the α -attractor dark energy model and the oscillatory tracker dark energy model. The background equations which determine the dynamics of the dark energy model is described in section 3. After considering linear perturbation

around the Friedmann-Lemaitre-Robertson-Walker (FLRW) background in section 4, we move to section 5 where we describe the datasets and methodology used to constrain the parameters of the model, and we also quantify our results through 2D posterior, best-fit and mean values. The section 6 is dedicated to the study of the effect of the oscillatory tracker dark energy model on CMB temperature and polarization power spectra, matter power spectrum and $f\sigma_8$. Finally, in section 7 we discuss and conclude upon our results.

2 OSCILLATORY TRACKER DARK ENERGY MODEL

The α -attractors have been gaining attention in the context of dark energy due to their possibility of linking both the inflationary and the present accelerated expansion of the universe. Their predictions in the inflationary paradigm are in good agreement with the latest cosmological observations (Akrami et al. 2018), and as quintessence models, they can also produce late time accelerated expansion compatible with the present measurements (García-García et al. 2018). In this article, we focus on the minimally coupled α -attractor dark energy model with the Lagrangian density in the Einstein frame represented by,

$$\mathcal{L} = \sqrt{-g} \left[\frac{1}{2} M_p^2 R - \frac{\alpha}{(1 - \frac{\phi^2}{6})^2} \frac{(\partial\phi)^2}{2} - \alpha f^2 \left(\frac{\phi}{\sqrt{6}} \right) \right], \quad (1)$$

where M_p is the Planck mass, α is a parameter and αf^2 is the potential function dependent on the field ϕ which is measured in M_p units. Here the kinetic term is not canonical, but can be made canonical by a field redefinition $\varphi = \sqrt{6\alpha} \tanh^{-1} \left(\frac{\phi}{\sqrt{6}} \right)$. Now the Lagrangian density can be written as,

$$\mathcal{L} = \sqrt{-g} \left[\frac{1}{2} M_p^2 R - \frac{(\partial\varphi)^2}{2} - \alpha f^2(x) \right], \quad (2)$$

where $x = \tanh \left(\frac{\varphi}{\sqrt{6\alpha}} \right)$. This implies one can write the scalar field potential as $V(\varphi) = \alpha f^2 \left(\tanh \left(\frac{\varphi}{\sqrt{6\alpha}} \right) \right)$. Among the various realizations of α -attractor dark energy models studied in (Bag et al. 2018), we focused our attention on the oscillatory tracker model given by,

$$V(\varphi) = \alpha c^2 \cosh \left(\frac{\varphi}{\sqrt{6\alpha}} \right), \quad (3)$$

where the constants α and c are the free parameters. The schematic representation of the oscillatory dark energy model is shown in figure 1. For large values of $\frac{|\varphi|}{\sqrt{6\alpha}} \gg 1$, the oscillatory tracker potential has the asymptotic form, $V(\varphi) \simeq \alpha c^2 \exp \left(\frac{\varphi}{\sqrt{6\alpha}} \right)$. So initially, the oscillatory tracker potential behaves like an exponential potential which exhibits a very large initial basin of attraction and has been extensively studied in (Ratra & Peebles 1988; Ferreira & Joyce 1997, 1998; Barreiro et al. 2000). During this period the OTM tracks the background density fields. Due to this exponential tracker asymptote, the oscillatory tracker model can avoid the fine tuning problem which affects many models of dark energy. Moreover, it is also worth to note that in OTM, the initial density values of scalar field covering a range of more than 40 orders of magnitude at $z = 10^{12}$ can converge onto the

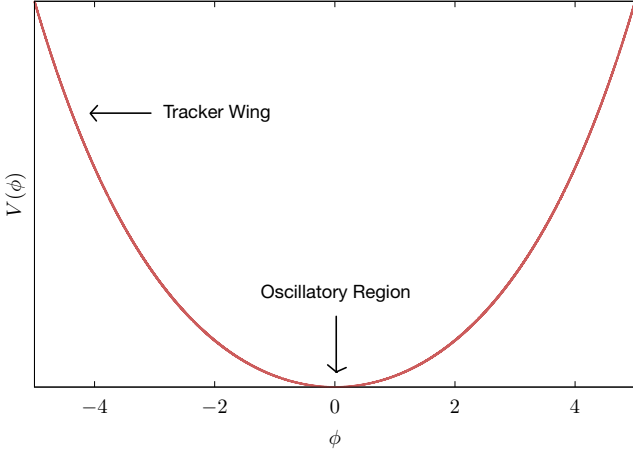


Figure 1. A schematic representation of the potential energy density for the oscillatory tracker dark energy model.

attractor scaling solution (Bag et al. 2018). This range substantially increases if we set our initial conditions at earlier times. Once the scalar field rolls down the exponential potential (tracker wing), it starts oscillating at the minimum of the potential (oscillatory region). For small values $\frac{|\varphi|}{\sqrt{6\alpha}} \ll 1$, the potential has the limiting form $V(\varphi) \simeq \alpha c^2 (1 + \frac{1}{2} (\frac{\varphi}{\sqrt{6\alpha}})^2)$. As a result, at the late time, the oscillatory tracker potential behaves like a cosmological constant αc^2 . However, because of the presence of φ^2 term, the equation of state parameter of the scalar field approaches $\omega_\phi \simeq -1$ via small oscillations. Thus due to the presence of the exponential tracker asymptote, the oscillatory tracker model has a very large initial basin of attraction, trajectories from which get funneled into the late time attractor $\omega_\phi \simeq -1$. For the detailed theoretical study of the properties of this potential, we refer to the work in (Bag et al. 2018).

3 BACKGROUND EVOLUTION

In the spatially flat homogeneous and isotropic model of the universe, the space-time interval ds between two events in a global comoving cartesian coordinate system is described by,

$$ds^2 = a^2(\tau)(-d\tau^2 + \delta_{ij}dx^i dy^j), \quad (4)$$

where τ represents the conformal time which is related to the comoving time t as $a^2 d\tau^2 = dt^2$ and $a(\tau)$ is the scale factor of expansion which satisfies the Friedmann equation,

$$\mathcal{H}^2 \equiv \left(\frac{a'}{a}\right)^2 = \frac{8\pi G}{3} a^2 \rho_{tot} = \frac{8\pi G}{3} a^2 (\rho_\gamma + \rho_\nu + \rho_b + \rho_c + \rho_\varphi), \quad (5)$$

where ρ_{tot} is the total background energy density of all species namely photons (γ), neutrinos (ν), baryons (b), cold dark matter (c) and a scalar field (φ) with a potential $V(\varphi)$ acting as dark energy. In this article, we use $c = 1$, reduced Planck mass $M_p = 1$ and the prime ($'$) represents derivative with respect to the conformal time τ . The equation of state parameter is given by $\omega_i = \frac{p_i}{\rho_i}$ where p_i corresponds to

the pressure of each species. For the photons and neutrinos, $\omega_\gamma = \omega_\nu = 1/3$, whereas for baryons and cold dark matter, $\omega_b = \omega_c = 0$. The background energy density and pressure for the scalar field are,

$$\rho_\varphi = \frac{1}{2a^2} \varphi'^2 + V(\varphi), \quad (6)$$

$$p_\varphi = \frac{1}{2a^2} \varphi'^2 - V(\varphi). \quad (7)$$

Using Eq. 6 and Eq. 7 the equation of state parameter of the scalar field reads,

$$\omega_\varphi = \frac{p_\varphi}{\rho_\varphi} = \frac{\frac{1}{2a^2} \varphi'^2 - V(\varphi)}{\frac{1}{2a^2} \varphi'^2 + V(\varphi)}. \quad (8)$$

The background Klein-Gordon equation can be obtained as a consequence of the Bianchi identities as

$$\varphi'' + 2\mathcal{H}\varphi' + a^2 \frac{dV}{d\varphi} = 0. \quad (9)$$

The evolution of the energy density parameters of radiation Ω_r where ($r = \gamma + \nu$), matter Ω_m where ($m = b + c$) and scalar field Ω_ϕ with the logarithmic of scale factor is shown in figure 2. The scalar field tracks both the background fields (r, m) at the early epochs and in the recent era it dominates over the background fields.

4 LINEAR PERTURBATIONS

In order to study the observational effects of the α -attractor dark energy models on the CMB and large scale structure, we need to consider linear perturbations around the FLRW background. The scalar perturbation of the FLRW metric takes the form (Väliiviita et al. 2008),

$$ds^2 = a^2(\tau) \left[- (1 + 2\Phi) d\tau^2 + 2\partial_i B d\tau dx^i + ((1 - 2\psi)\delta_{ij} + 2\partial_i \partial_j E) dx^i dx^j \right], \quad (10)$$

where Φ, ψ, B, E are gauge-dependent functions of both space and time. In synchronous gauge $\Phi = B = 0$, $\psi = \eta$ and $k^2 E = -h/2 - 3\eta$, where η and h are the synchronous gauge fields defined in the Fourier space and k is the wave number (Ma & Bertschinger 1995). In Fourier space, the perturbation equations in the matter sector reads as,

$$\delta'_i + k v_i + \frac{h'}{2} = 0, \quad (11)$$

$$v'_i + \mathcal{H}v_i = 0, \quad (12)$$

where $\delta_i = \delta\rho_i/\rho_i$ is the density contrast and v_i is the peculiar velocity of i -th ($i = b, c$) fluid. Assuming there is no momentum transfer in CDM frame, we set v_c to zero. For the details of these sets of equation, we refer to the works of (Ma & Bertschinger 1995; Kodama & Sasaki 1984; Mukhanov et al. 1992; Malik et al. 2003). The linearized scalar field equation in the Fourier space with wave number k is given by,

$$\delta\varphi'' + 2\mathcal{H}\delta\varphi' + k^2\delta\varphi + a^2 \frac{d^2V}{d\varphi^2} \delta\varphi + \frac{1}{2}\varphi' h' = 0, \quad (13)$$

where $V(\varphi)$ is the potential energy density corresponding to the oscillatory model given in Eq. 3. The perturbation in the

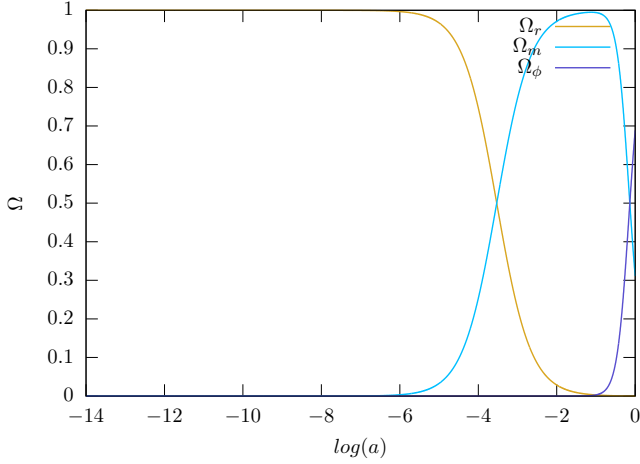


Figure 2. Figure showing the variation of density parameter Ω as a function of scale factor, a . Here the radiation density Ω_r and matter density Ω_m are plotted along with scalar field density Ω_ϕ .

energy density $\delta\rho_\phi$ and pressure δp_ϕ are,

$$\delta\rho_\phi = -\delta T_{0(\varphi)}^0 = \frac{\varphi'\delta\varphi'}{a^2} + \delta\varphi\frac{dV}{d\varphi}, \quad (14)$$

$$\delta T_{0(\varphi)}^j = -\frac{ik_j\varphi'\delta\varphi}{a^2}, \quad (15)$$

$$\delta p_\phi\delta_j^i = \delta T_{j(\varphi)}^i = \left(-\frac{\varphi'\delta\varphi'}{a^2} - \delta\varphi\frac{dV}{d\varphi}\right)\delta_j^i, \quad (16)$$

here $\delta T_{j(\varphi)}^i$ is the perturbed stress-energy tensor of the scalar field. For an adiabatically expanding universe, the square of sound speed is $c_{s,\varphi}^2 = p'_\phi/\rho'_\phi$. We implemented the above equations in CLASS (Blas et al. 2011; Lesgourgues 2011) with adiabatic initial conditions in order to compute the CMB temperature and polarization power spectra and matter power spectrum.

5 OBSERVATIONAL CONSTRAINTS

In this section, we compare the oscillatory tracker model with recent observational data. The motivation of this section is to obtain the best-fit and mean values of the cosmological parameters when the oscillatory tracker model is taken into account. In section 5.1, we explain the datasets used to constrain the parameters of the model. The analysis of these datasets will help us to accurately determine the implications of the oscillatory tracker model on the CMB power spectra, matter power spectrum and the $f\sigma_8$, which we plan to study in the next section.

5.1 Data Sets

CMB:- The data from CMB is very powerful in constraining the dark energy models. Here we used the latest CMB data from the Planck 2018 final data release (Planck Collaboration et al. 2020). The CMB likelihood consists of the low- ℓ temperature likelihood, C_ℓ^{TT} , low- ℓ polarization likelihood, C_ℓ^{EE} , high- ℓ temperature-polarization likelihood, C_ℓ^{TE} and high- ℓ combined TT, TE and EE likelihood. The low- ℓ CMB

Parameter	Prior
$\Omega_b h^2$	[0.005, 0.1]
$\Omega_c h^2$	[0.001, 0.99]
τ_{reio}	[0.01, 0.8]
H_0	[20, 100]
n_s	[0.8, 1.2]
$\log(10^{10} A_s)$	[1.61, 3.91]
φ_i	10
$10^5 c$	[0.01, 1.0]
α	[0.0, 10.0]

Table 1. The range of priors used for MCMC analysis.

likelihood covers the multipole range $2 \leq \ell \leq 29$ whereas the high- ℓ likelihood spans the multipole range $\ell \geq 30$.

Type 1a supernovae:- The type 1a supernovae, considered standard candles, is an ideal probe for studying cosmological expansion. In this article, we consider the type 1a supernovae data from the Pantheon compilation (Scolnic et al. 2018). This consists of 1048 type 1a supernovae data points distributed in the redshift interval $0.01 < z < 2.26$.

BAO:- The fluctuations in the photon-baryon fluid in the early universe leave their imprints as acoustic peaks in the CMB angular power spectrum. These anisotropies in the baryon acoustic oscillations provide tighter constraints on the cosmological parameters. Here we consider the BAO data from different astronomical surveys 6dFGS (Beutler et al. 2011), BOSS DR12 (Alam et al. 2017) and SDSS main galaxy sample (Ross et al. 2015).

5.2 Methodology and Posterior Analysis

The posterior distribution for the oscillatory tracker model is obtained by sampling the parameter space with a Markov Chain Monte Carlo method (MCMC). In particular, to obtain the best-fit and the mean values of the cosmological parameters, we make use of MCMC simulator Cobaya (Torrado & Lewis 2021) and a modified version of the CLASS (Blas et al. 2011; Lesgourgues 2011). For the statistical analysis of the MCMC results, we make use of the publicly available GetDist (Lewis 2019) software package. We sample the posterior parameter distribution until the Gelman-Rubin convergence statistic (Gelman & Rubin 1992) satisfies $R - 1 < 0.01$. The parameter space for constraining the oscillatory tracker dark energy model is,

$$P \equiv [\Omega_b h^2, \Omega_c h^2, H_0, n_s, \tau_{reio}, \ln(10^{10} A_s), \alpha, 10^5 c],$$

where $\Omega_b h^2$ is the baryon density, $\Omega_c h^2$ is the cold dark matter density, τ_{reio} is the optical depth to reionization, H_0 is the Hubble constant, A_s is the scalar primordial power spectrum amplitude, n_s is the scalar spectral index and α and c are the free model parameters. Moreover, the initial condition for the scalar field velocity $\dot{\varphi}_i$ is set to zero, and since, the same results are obtained for the different initial values of the scalar field φ_i , we fixed the scalar field initial value φ_i to be 10. The parameter space, P for the oscillatory model is explored for the flat prior ranges given in table 1.

The posterior distributions for the parameters of the oscillatory tracker model are shown in figure 3. The contours show

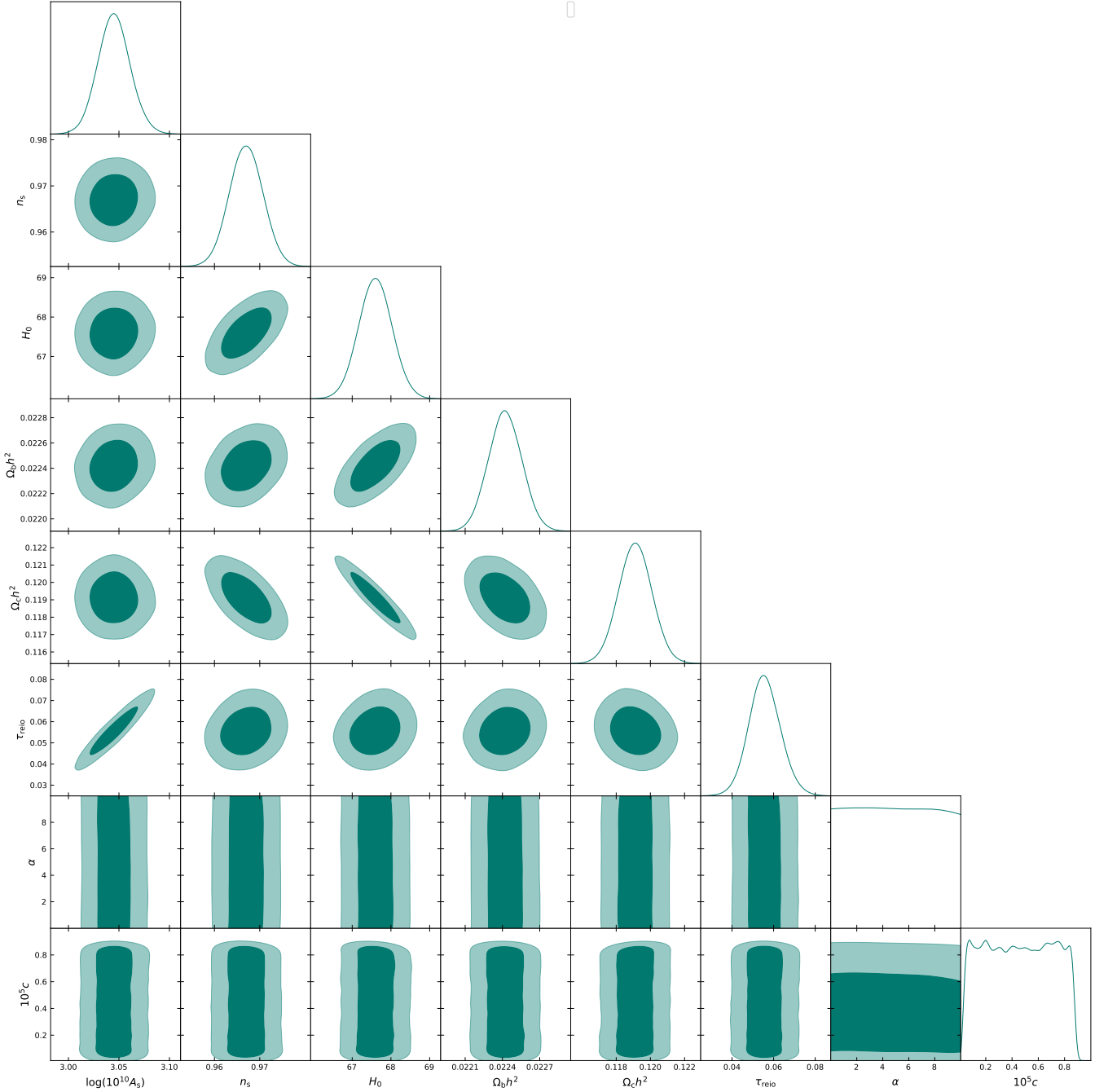


Figure 3. The posterior distribution for the model parameters of the OTM. The contours show 68.3% and 95.5% confidence regions. A noticeable correlation exists between the parameter pairs $(H_0, \Omega_c h^2)$ and $(\tau_{reio}, \log(10^{10} A_s))$. The other parameter pairs $(\Omega_b h^2, H_0)$, $(\Omega_c h^2, n_s)$ and $(\Omega_c h^2, \Omega_b h^2)$ also exhibit minor degree of correlations. The quantitative results are summarised in table 2.

1σ region of 68% confidence level and 2σ region of 95% confidence level with the darker colour signifying the more probable results. From the quantitative results summarized in table 2, it is interesting to note that the standard cosmological parameters of the oscillatory tracker model are in good agreement with the LCDM Planck 2018 results (Aghanim et al. 2020) given in table 3. This signifies the fact that the OTM has a close resemblance to the usual LCDM model. However, we observe that the amount of cold dark matter $\Omega_c h^2$ for the

oscillatory tracker model is comparatively lower than the base LCDM model. This slight decrease in the amount of matter content of the universe has a direct effect on the CMB sector and matter sector, which we further investigate in section 6. It is also worth to note that the hubble parameter value H_0 for oscillatory tracker model is consistent with LCDM Planck 2018 results ($H_0 = (67.27 \pm 0.6) \text{ Km s}^{-1} \text{ Mpc}^{-1}$) within 1σ . Moreover, the flat posteriors for the model parameters α and c indicate that, there is a broad range of parameter values

Parameter	Best-fit \pm 95.5% limits	Mean \pm 95.5% limits
$\Omega_b h^2$	$0.02243^{+0.00056}_{-0.00045}$	0.02242 ± 0.00026
$\Omega_c h^2$	$0.1192^{+0.0038}_{-0.0040}$	0.1191 ± 0.0019
n_s	$0.9672^{+0.014}_{-0.015}$	0.9670 ± 0.0072
H_0	$67.474^{+1.86}_{-1.60}$	$67.5989^{+0.8498}_{-0.8401}$
$\ln(10^{10} A_s)$	$3.0417^{+0.075}_{-0.057}$	$3.0452^{+0.0324}_{-0.0308}$
τ_{reio}	$0.05247^{+0.036}_{-0.028}$	$0.0557^{+0.0157}_{-0.0148}$
α	$5.5983^{+4.40}_{-5.59}$	$4.972^{+4.972}_{-5.028}$
$10^5 c$	$0.52199^{+0.390}_{-0.496}$	$0.4546^{+0.4006}_{-0.4052}$

Table 2. Best-fit and mean values with 95.5% intervals for the parameters of the oscillatory tracker model. Both best-fit and mean values of the parameters except α and $10^5 c$ agree very well with each other. H_0 units are $\text{km s}^{-1} \text{Mpc}^{-1}$ and Mpc^{-2} for c^2 .

Parameter	Mean \pm 68% limits (Planck 2018)
$\Omega_b h^2$	0.02236 ± 0.00015
$\Omega_c h^2$	0.1201 ± 0.0014
n_s	0.9649 ± 0.0044
H_0	67.27 ± 0.60
$\ln(10^{10} A_s)$	3.045 ± 0.016
τ_{reio}	$0.0544^{+0.0070}_{-0.0081}$

Table 3. The mean values with 68% intervals for the parameters of the LCDM model from Planck 2018 (Aghanim et al. 2020). The LCDM values agree excellently with the corresponding parameter values of OTM case shown in table 2.

for α and c for which the OTM is consistent with the set of observational data presented in section 5.1.

6 EFFECTS ON OBSERVABLE PROBES

In this section, in order to study the impact of oscillatory tracker dark energy model on different observable quantities, we focus on its effects on CMB power spectra (TT, EE, TE), matter power spectrum and $f\sigma_8$. For this analysis, we make use of the modified version of the public available boltzmann code CLASS (Blas et al. 2011; Lesgourgues 2011) with the best-fit values of the cosmological parameters from table 2. On the other hand, for the case of the LCDM model, we implement the cosmological parameter values from Planck 2018 data (Aghanim et al. 2020) (see table 3) in CLASS and hereon, the LCDM model is our base model.

6.1 CMB Sector

The CMB radiation has a significant role in understanding our universe as its an open window to the early universe. This radiation field is nearly isotropic and exhibits almost a perfect black body spectrum at a temperature of $2.73K$ (Aghanim

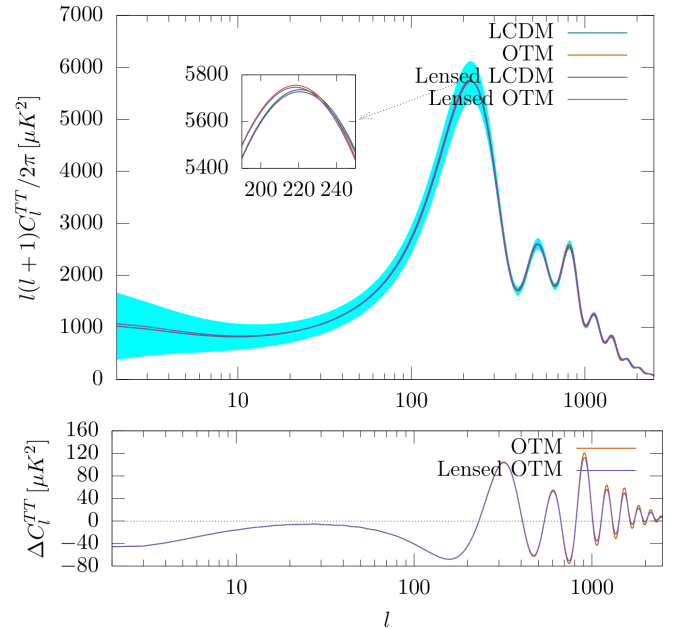


Figure 4. Top panel: Figure showing the comparison of CMB temperature (TT) power spectrum of OTM with respect to the base LCDM model for both lensed and unlensed cases. The inset shows the zoomed-in versions of the peak and the cyan band represents the cosmic variance corresponding to C_l^{TT} of LCDM. Due to the presence of the scalar field, the peak positions of OTM power spectrum are marginally higher than the base LCDM. Bottom Panel: Figure showing the deviations of the CMB TT power spectrum of the OTM from the base LCDM for both lensed and unlensed cases.

et al. 2020). The numerical evaluation of CMB temperature and polarization power spectra is implemented in the CLASS code. The comparison of CMB TT power spectrum of oscillatory tracker model with respect to base LCDM is shown with and without lensing effects in the top panel of figure 4. Here the inset shows the zoomed-in versions of the first peak of the CMB TT power spectrum. From our analysis of oscillatory tracker model with the observational datasets given in section 5.1, we find that the cold dark matter density $\Omega_c h^2$ for OTM is slightly lower than the base LCDM model (see table 2 and table 3).

The amount of dark matter plays a significant role in determining the time at which the universe transitioned from radiation-dominated epoch to matter-dominated epoch. So a lower dark matter density in the oscillatory tracker model results in delaying this transition epoch. As a result, the universe enters matter domination later compared to the usual LCDM model. As the universe becomes more radiation dominated in the early phases of the evolution of OTM, it affects the gravitational potential wells. It thus causes an increase in the so-called 'radiation driving effect' (Hu & Dodelson 2002) which manifests as a rise in the acoustic peaks of the CMB power spectrum. Due to this driving effect, the peak positions of the CMB TT power spectrum for the oscillatory tracker model is marginally higher than the base LCDM model (see bottom panel of the figure 4). The presence of the scalar field also increases the low- l modes of the CMB TT power spectrum through the Integrated Sachs-Wolfe (ISW) effect.

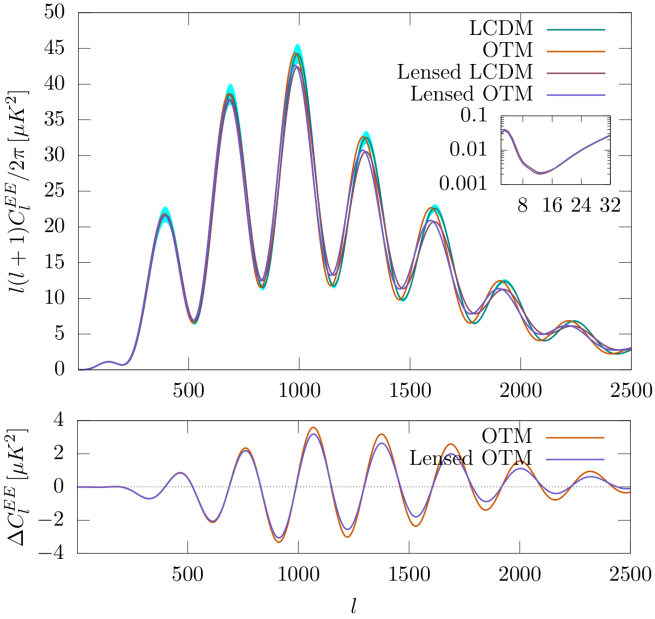


Figure 5. Top panel: Figure showing the comparison of CMB polarization (EE) power spectrum of OTM with respect to the base LCDM model for both lensed and unlensed cases. The inset shows the zoomed-in versions of the low- ℓ modes, and the cyan band represents the cosmic variance corresponding to C_l^{EE} of LCDM. The peak positions of both OTM and LCDM are slightly lowered when the lensing effects are taken into account, and its effects are noticeably higher at higher multipoles. Bottom panel: Figure showing the deviations of CMB polarization (EE) power spectrum from the base LCDM for both lensed and unlensed cases.

Moreover, with matter-radiation equality occurring later in OTM, the decay of the gravitational potentials goes further beyond the decoupling. As a result, the stronger ISW effects also contribute coherently to the height of the first peak (see inset of figure 4). As the cosmic variance is larger in the lower multipole regions, the additional effects introduced by the scalar field is difficult to distinguish from the predictions of the LCDM model. It will be an interesting future work to observationally detect such minor changes for the case of OTM from the LCDM predictions in the cosmic variance dominated low multipole regions. The bottom panel of figure 4 shows the deviations of the CMB TT power spectrum of the oscillatory tracker model from the base LCDM model for both lensed and unlensed cases. It is evident that the deviations of OTM from the LCDM are dominant at the acoustic peaks, and it decreases for higher multipoles ranges.

The comparison of CMB EE and TE power spectra of oscillatory tracker dark energy model with respect to the base LCDM model is shown with and without lensing effects in figure 5 and figure 6 respectively. The polarization peaks are at the troughs of the CMB temperature power spectrum. The effects of scalar field on the low- ℓ modes of the CMB EE power spectrum is shown in the inset in the figure 5. As the low- ℓ modes of EE power spectrum of OTM closely match LCDM, the reionization history in both models are not altered to a great extent. This is due to the fact that the optical depth to the reionization τ_{reio} for OTM (see table 2) is consistent with LCDM Planck 2018 (Aghanim et al. 2020) within

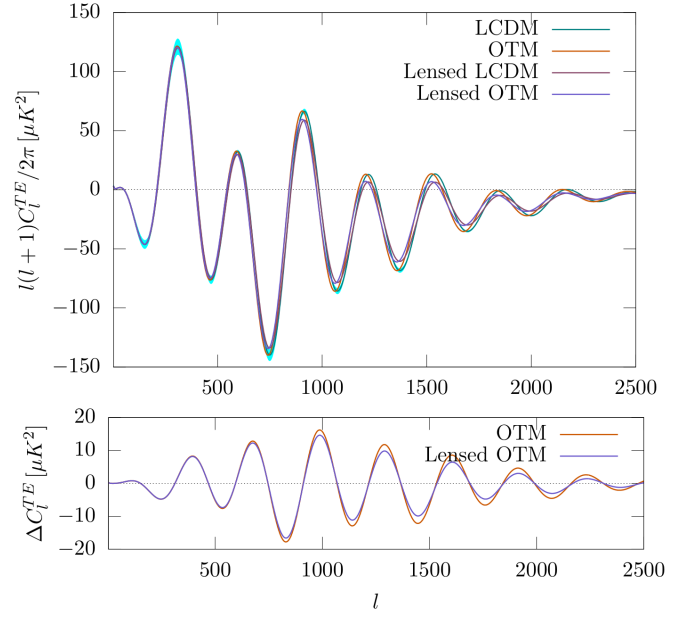


Figure 6. Top panel: Figure showing the comparison of CMB temperature-polarization (TE) power spectrum of OTM with respect to the base LCDM model for both lensed and unlensed cases. The cyan band represents the cosmic variance corresponding to C_l^{TE} of LCDM. The lensing effects slightly reduce the peak positions of the CMB TE power spectrum, and the effects are noticeably higher at higher multipoles. Bottom panel: Figure showing the CMB TE power spectrum deviations from the base LCDM for lensed and unlensed cases.

1σ . The peak heights of CMB temperature and polarization power spectra are marginally lowered when the lensing effects are considered. Moreover, it is also visible that the effect of lensing is noticeably higher at higher multipoles.

6.2 Matter Sector

The observed cosmic structures are the results of the amplification of primordial density fluctuations by gravitational instability. The power spectrum of matter density fluctuations plays a significant role in understanding the dynamics of our universe. The matter power spectrum (Dodelson 2003) can be written as,

$$P(k, a) = A_s k^{n_s} T^2(k) D^2(a), \quad (17)$$

where A_s is the scalar primordial power spectrum amplitude, $T(k)$ is the matter transfer function, n_s is the spectral index and $D(a) = \frac{\delta_m(a)}{\delta_m(a=1)}$ is the normalized density contrast. The combined effects of the complementary actions of the outward push by the radiation pressure and the inward pull by the gravity, which are responsible for the acoustic oscillations in the CMB, also determine the power spectrum of non-relativistic matter. From our analysis of the oscillatory tracker model with observational datasets given in section 5.1, we find that because of the presence of scalar field; there is a minor decrease in the amount of cold dark matter $\Omega_c h^2$ present in the universe compared to the base LCDM model (see table 2 and table 3). A decrease in the matter content of the universe in turn, reduces the matter power spec-

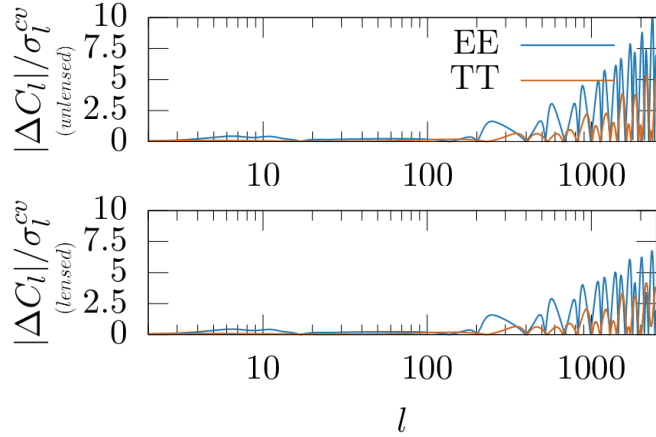


Figure 7. Top panel: Figure showing the fraction of absolute difference of CMB angular power spectra (TT and EE) between the OTM and LCDM models with the LCDM predicted cosmic variance errors without CMB weak lensing taken into considerations. Bottom panel: Same as top panel, but power spectra are obtained taking into account CMB lensing effects as well. Rapidly increasing deviations between the OTM and LCDM models are predicted at larger multipoles at the locations of peaks and troughs of the acoustic oscillations of the two spectra. Comparing both TT and EE, it is interesting to note that the fractional change for the case of EE is somewhat larger than the TT case at large multipoles.

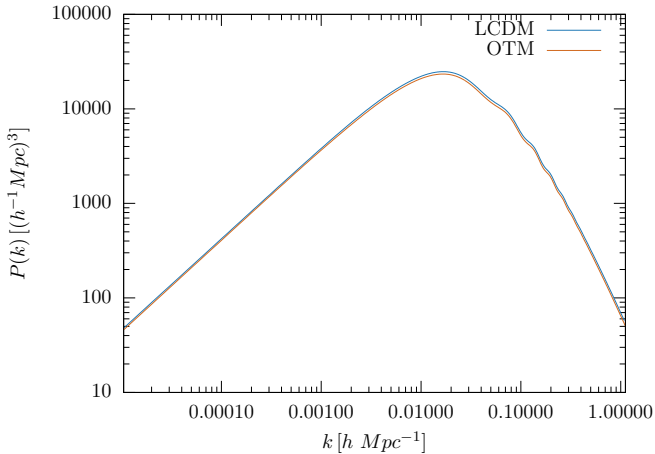


Figure 8. The figure showing the variation of matter power spectrum $P(k)$ as a function of comoving wave number k for both OTM and base LCDM model. The presence of scalar field slightly reduces the matter content of the universe; as a result, the matter power spectrum of OTM is slightly lower than the base LCDM model.

trum compared to the base LCDM model. This effect of the scalar field that decreases matter power spectrum is shown in figure 8. Any dynamical effect that reduces the amplitude of the matter power spectrum corresponds to a decay in the Newtonian potential that boosts the level of anisotropy (Hu & Dodelson 2002). Thus a decrease in the matter content of the universe due to the presence of scalar field drives the matter power spectrum down and the CMB spectrum up.

Another great tool to differentiate various dark energy models based on the growth of large scale structures is the

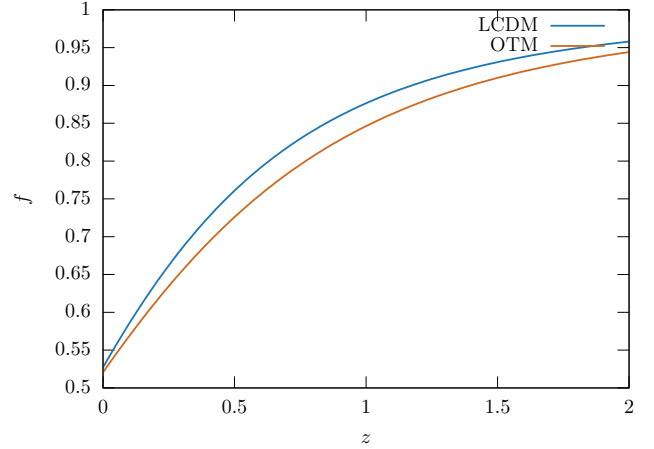


Figure 9. Figure showing the variation of linear growth rate f as a function of redshift z in the low redshift regime. The linear growth rate for OTM is slightly lower compared to the base LCDM model.

linear growth rate. One can define the linear growth rate as,

$$f(a) = \frac{d \ln \delta_m}{d \ln a} = \frac{a}{\delta_m(a)} \frac{d \delta_m}{d a}. \quad (18)$$

A more powerful and dependable observational quantity that is measured by redshift surveys is the product of $f(a)\sigma_8$ (Percival & White 2009), where σ_8 is the root-mean-square (rms) fluctuations of the linear density field within the sphere of radius $R = 8 h^{-1} \text{Mpc}$. In the linear regime, σ_8 and $f\sigma_8$ can be read as (Nesseris & Perivolaropoulos 2008; Song & Percival 2009; Huterer et al. 2015; Ishak 2018),

$$\sigma_8(z) = \sigma_8(z=0) \frac{\delta_m(z)}{\delta_m(z=0)}, \quad (19)$$

and

$$f\sigma_8(z) \equiv f(z)\sigma_8(z) = -(1+z) \frac{\sigma_8(z=0)}{\delta_m(z=0)} \frac{d\delta_m}{dz}, \quad (20)$$

where $\sigma_8(z=0)$ is the value of the rms fluctuations of the linear density field at $z=0$. The redshift z is related to the scale factor a as $z = \frac{a_0}{a} - 1$ where a_0 is the present value of the scale factor. We obtained the σ_8 value (see table 4) of OTM using the best-fit parameters given in table 2 whereas for LCDM model we used the mean values given in table 3. As $f\sigma_8$ is a more reliable quantity (Percival & White 2009), it gives a better insight into the growth of the density perturbations. At low redshift, both the linear growth rate f and $f\sigma_8$ are independent of the wave number k . So we consider the redshift in the ranges $z=0$ to $z=2$. The variation of the linear growth rate and $f\sigma_8$ as a function of redshift z is shown in figure 9 and figure 10 respectively. The linear growth rate for the case of the oscillatory dark energy model is slightly lower than the base LCDM model. Both linear growth rate f and $f\sigma_8$ are lower for the oscillatory model at redshift $z=0$. The difference in the matter power spectrum is manifested in the amplitude of σ_8 given in table 4 and hence in $f\sigma_8$ shown in figure 10. Moreover, the lower value of σ_8 in OTM also results in the reduction of the clustering of galaxies compared to base LCDM.

Model	σ_8
OTM	0.7939
LCDM	0.8231

Table 4. The values of σ_8 at redshift $z = 0$ for the OTM and the LCDM model.

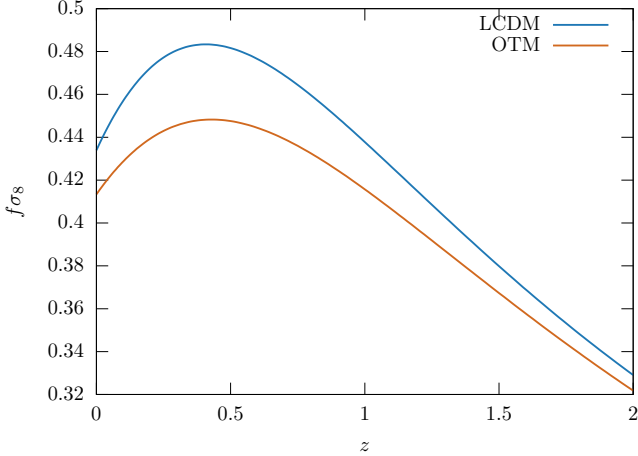


Figure 10. Figure showing the variation of $f\sigma_8$ as a function of redshift z in the low redshift regime. At the present epoch $z = 0$, the $f\sigma_8$ of OTM is lower than the base LCDM model.

7 CONCLUSION

The dark energy models with tracker properties have gained great attention over the years because of their ability to alleviate the cosmic coincidence problem. In this scenario, the scalar field which drives the accelerated expansion of the universe can reach the present value of dark energy density from a wide range of initial conditions. In this work, we investigated and extended the study of the oscillatory tracker dark energy model (Cedeño et al. 2019), which belongs to a family of tracking dark energy models known as α -attractors against various observational data consisting of CMB, BAO and type 1a supernovae data. The oscillatory tracker dark energy model, which is very much favoured over other α -attractor dark energy models (Cedeño et al. 2019) has a large initial attractor basin. As a result, the present observed dark energy density can be obtained from a very large range of initial conditions, which provides a solution to the so-called ‘fine-tuning’ problem.

By comparing the OTM against various observational data (CMB, BAO, type 1a supernovae), we constrained the parameters of the model in section 5. From the quantitative results given in table 2, it is interesting to note that the standard cosmological parameters are in good agreement with the LCDM Planck 2018 results (Aghanim et al. 2020). This signifies the fact that the OTM has a close resemblance to the usual LCDM model. Moreover, the flat posteriors of the parameters of oscillatory tracker model α and c indicate that there is a broad range of allowed values for these parameters for which the OTM is consistent with the set of observational data presented in section 5.1.

After obtaining the best-fit model parameters, in section 6

we investigated the effect of the OTM on CMB temperature and polarization power spectra, matter power spectrum and the $f\sigma_8$. Though the oscillatory tracker model and usual LCDM are qualitatively very similar, they are not really overlapping. The less dark matter content in the oscillatory tracker model leads to a later epoch of matter-radiation equality and more decay of gravitational potentials. This causes an increase in the radiation driving effects and results in the rise of the amplitudes of the acoustic peaks in the oscillatory tracker model. The fraction of absolute difference of CMB angular power spectra (TT and EE) between OTM and LCDM models with the LCDM predicted cosmic variance errors also suggest an increase in the deviations at larger multipoles at the locations of peaks and troughs of the acoustic oscillations of the two spectra. The effect of the decrease in matter content of the universe due to the presence of the scalar field is also seen as a decrease in the power of matter power spectrum compared to the base LCDM model. The comparison between the CMB and the large scale structure is important, since it breaks the degeneracies between effects due to deviations from power law initial conditions and the dynamics of the matter and energy content of the universe (Hu & Dodelson 2002). Any dynamical effect which reduces the matter power spectrum corresponds to the decay of gravitational potential wells that boosts the amplitude of the acoustic peaks in the CMB power spectrum. As a result, the decrease in matter content of the universe in OTM drives the matter power spectrum down and the CMB power spectrum up. Moreover, our investigation on the linear growth rate f and $f\sigma_8$ at a low redshift regime indicates that the f and $f\sigma_8$ are slightly lower than the base LCDM model. The lower value of σ_8 of the oscillatory tracker dark energy model signifies that the presence of scalar field reduces the galaxy clustering compared to the base LCDM model.

Our analysis on the CMB sector and matter sector suggest that the oscillatory tracker dark energy model can be equally viable to the usual LCDM model given the current set of observational data used in this work. It will be interesting to investigate the future generation more sensitive observations like HETDEX (Hill et al. 2008), WFIRST (Spergel et al. 2015) and LSST (Ivezić et al. 2019) in detail so as to detect the small differences between the OTM and LCDM models reported in this article in order to constrain the models further.

ACKNOWLEDGEMENTS

Computations were carried out on Kanad, the high performance computation facility of IISER Bhopal, India. AJ acknowledges financial support from the Ministry of Human Resource and Development, Government of India via Institute fellowship at IISER Bhopal.

8 DATA AVAILABILITY

The data underlying this article will be shared on reasonable request to the corresponding author.

REFERENCES

- Abazajian K., et al., 2015, *Astroparticle Physics*, 63, 55–65
- Abramo L., Finelli F., 2003, *Physics Letters B*, 575, 165–171
- Aghanim N., et al., 2020, *Astronomy & Astrophysics*, 641, A6
- Aguirregabiria J., Lazkoz R., 2004, *Physical Review D*, 69
- Akrami Y., Kallosh R., Linde A., Vardanyan V., 2018, *Journal of Cosmology and Astroparticle Physics*, 2018, 041–041
- Alam S., et al., 2017, *MNRAS*, 470, 2617
- Armendariz-Picon C., Mukhanov V., Steinhardt P. J., 2000, *Physical Review Letters*, 85, 4438–4441
- Armendariz-Picon C., Mukhanov V., Steinhardt P. J., 2001, *Physical Review D*, 63
- Bag S., Mishra S. S., Sahni V., 2018, *Journal of Cosmology and Astroparticle Physics*, 2018, 009–009
- Bagla J. S., Jassal H. K., Padmanabhan T., 2003, *Physical Review D*, 67
- Barreiro T., Copeland E. J., Nunes N. J., 2000, *Phys. Rev. D*, 61, 127301
- Beutler F., et al., 2011, *MNRAS*, 416, 3017
- Beutler F., Blake C., Koda J., Marín F. A., Seo H.-J., Cuesta A. J., Schneider D. P., 2015, *Monthly Notices of the Royal Astronomical Society*, 455, 3230–3248
- Bezrukov F., Shaposhnikov M., 2008, *Physics Letters B*, 659, 703–706
- Blake C., et al., 2012, *Monthly Notices of the Royal Astronomical Society*, 425, 405–414
- Blas D., Lesgourgues J., Tram T., 2011, *Journal of Cosmology and Astroparticle Physics*, 2011, 034–034
- Brax P., Davis A.-C., 2015, *Journal of Cosmology and Astroparticle Physics*, 2015, 042–042
- Brown J., Cottrell W., Shiu G., Soler P., 2016, *Journal of High Energy Physics*, 2016
- Caldwell R., 2002, *Physics Letters B*, 545, 23–29
- Caldwell R. R., Kamionkowski M., Weinberg N. N., 2003, *Physical Review Letters*, 91
- Cedeño F. X. L., Montiel A., Hidalgo J. C., German G., 2019, *Journal of Cosmology and Astroparticle Physics*, 2019, 002–002
- Cervantes-Cota J., Dehnen H., 1995, *Nuclear Physics B*, 442, 391–409
- Chiba T., Okabe T., Yamaguchi M., 2000, *Physical Review D*, 62
- Chiba T., De Felice A., Tsujikawa S., 2013, *Physical Review D*, 87
- Clifton T., Ferreira P. G., Padilla A., Skordis C., 2012, *Physics Reports*, 513, 1–189
- Conlon J. P., 2012, *Journal of Cosmology and Astroparticle Physics*, 2012, 033–033
- Copeland E. J., Garousi M. R., Sami M., Tsujikawa S., 2005, *Physical Review D*, 71
- Damour T., Piazza F., Veneziano G., 2002, *Physical Review Letters*, 89
- Dimitrijevic I., Dragovich B., Grujic J., Rakic Z., 2013, *Lie Theory and Its Applications in Physics*, p. 251–259
- Dodelson S., 2003, *Modern Cosmology*
- Durrive J.-B., Ooba J., Ichiki K., Sugiyama N., 2018, *Physical Review D*, 97
- Eisenstein D. J., et al., 2005, *The Astrophysical Journal*, 633, 560–574
- Ferrara S., Kallosh R., Linde A., Marrani A., Van Proeyen A., 2010, *Phys. Rev. D*, 82, 045003
- Ferreira P. G., Joyce M., 1997, *Phys. Rev. Lett.*, 79, 4740
- Ferreira P. G., Joyce M., 1998, *Phys. Rev. D*, 58, 023503
- Flauger R., McAllister L., Pajer E., Westphal A., Xu G., 2010, *Journal of Cosmology and Astroparticle Physics*, 2010, 009–009
- García-García C., Linder E. V., Ruiz-Lapuente P., Zumalacárregui M., 2018, *Journal of Cosmology and Astroparticle Physics*, 2018, 022–022
- Gelman A., Rubin D. B., 1992, *Statist. Sci.*, 7, 457
- Goncharov A. S., Linde A. D., 1984a, *Sov. Phys. JETP*, 59, 930
- Goncharov A. B., Linde A. D., 1984b, *Phys. Lett. B*, 139, 27
- Guo Z.-K., Zhang Y.-Z., 2004, *Journal of Cosmology and Astroparticle Physics*, 2004, 010–010
- Guth A. H., 1981, *Phys. Rev. D*, 23, 347
- Hill G. J., et al., 2008, The Hobby-Eberly Telescope Dark Energy Experiment (HETDEX): Description and Early Pilot Survey Results ([arXiv:0806.0183](https://arxiv.org/abs/0806.0183))
- Hinshaw G., et al., 2013, *The Astrophysical Journal Supplement Series*, 208, 19
- Hu W., Dodelson S., 2002, *Annual Review of Astronomy and Astrophysics*, 40, 171–216
- Huterer D., et al., 2015, *Astroparticle Physics*, 63, 23–41
- Ishak M., 2018, *Living Reviews in Relativity*, 22
- Ivezić et al., 2019, *The Astrophysical Journal*, 873, 111
- Joyce A., Lombriser L., Schmidt F., 2016, *Annual Review of Nuclear and Particle Science*, 66, 95–122
- Kaiser D. I., Sfakianakis E. I., 2014, *Physical Review Letters*, 112
- Kallosh R., Linde A., 2013, *Journal of Cosmology and Astroparticle Physics*, 2013, 002–002
- Kallosh R., Linde A., Roest D., 2013, *Journal of High Energy Physics*, 2013
- Kallosh R., Linde A., Roest D., 2014, *Journal of High Energy Physics*, 2014
- Kazin E. A., et al., 2014, *Monthly Notices of the Royal Astronomical Society*, 441, 3524–3542
- Kodama H., Sasaki M., 1984, *Progress of Theoretical Physics Supplement*, 78, 1
- Kofman L. A., Linde A. D., Starobinsky A. A., 1985, *Phys. Lett. B*, 157, 361
- Lesgourgues J., 2011, The Cosmic Linear Anisotropy Solving System (CLASS) I: Overview ([arXiv:1104.2932](https://arxiv.org/abs/1104.2932))
- Lewis A., 2019, GetDist: a Python package for analysing Monte Carlo samples ([arXiv:1910.13970](https://arxiv.org/abs/1910.13970))
- Li M., Li X.-D., Wang S., Wang Y., 2011, *Communications in Theoretical Physics*, 56, 525–604
- Linde A. D., 1982, *Phys. Lett. B*, 108, 389
- Linde A. D., 1983, *Phys. Lett. B*, 129, 177
- Linde A., 2015, *Journal of Cosmology and Astroparticle Physics*, 2015, 030–030
- Linde A., Noorbala M., Westphal A., 2011, *Journal of Cosmology and Astroparticle Physics*, 2011, 013–013
- Linder E. V., 2007, *General Relativity and Gravitation*, 40, 329–356
- Lobo F. S. N., 2008, The dark side of gravity: Modified theories of gravity ([arXiv:0807.1640](https://arxiv.org/abs/0807.1640))
- Ludwick K. J., 2018, *Phys. Rev. D*, 98, 043519
- L’Huillier B., Shafieloo A., Hazra D. K., Smoot G. F., Starobinsky A. A., 2018, *Monthly Notices of the Royal Astronomical Society*, 477, 2503–2512
- Ma C.-P., Bertschinger E., 1995, *ApJ*, 455, 7
- Malik K. A., Wands D., Ungarelli C., 2003, *Phys. Rev. D*, 67, 063516
- McAllister L., Silverstein E., Westphal A., 2010, *Physical Review D*, 82
- Miranda T., Fabris J. C., Piattella O. F., 2017, *Journal of Cosmology and Astroparticle Physics*, 2017, 041–041
- Mukhanov V. F., Chibisov G. V., 1981, *JETP Lett.*, 33, 532
- Mukhanov V. F., Feldman H. A., Brandenberger R. H., 1992, *Phys. Rep.*, 215, 203
- Nesseris S., Perivolaropoulos L., 2008, *Phys. Rev. D*, 77, 023504
- Nojiri S., Odintsov S. D., Tsujikawa S., 2005, *Physical Review D*, 71
- Padmanabhan T., 2002, *Physical Review D*, 66
- Parkinson D., et al., 2012, *Physical Review D*, 86
- Percival W. J., White M., 2009, *Monthly Notices of the Royal Astronomical Society*, 393, 297–308
- Perlmutter S., et al., 1999, *The Astrophysical Journal*, 517, 565–586

- Piazza F., Tsujikawa S., 2004, *Journal of Cosmology and Astroparticle Physics*, 2004, 004–004
- Planck Collaboration Aghanim N., et al., 2020, *A&A*, **641**, A5
- Ratra B., Peebles P. J. E., 1988, *Phys. Rev. D*, **37**, 3406
- Riess A. G., et al., 1998, *The Astronomical Journal*, **116**, 1009–1038
- Ross A. J., Samushia L., Howlett C., Percival W. J., Burden A., Manera M., 2015, *MNRAS*, **449**, 835
- Sahni V., 2002, *Classical and Quantum Gravity*, **19**, 3435–3448
- Salopek D. S., Bond J. R., Bardeen J. M., 1989, *Phys. Rev. D*, **40**, 1753
- Scolnic D. M., et al., 2018, *ApJ*, **859**, 101
- Shahalam M., Myrzakulov R., Myrzakul S., Wang A., 2018, *International Journal of Modern Physics D*, **27**, 1850058
- Silverstein E., Westphal A., 2008, *Phys. Rev. D*, **78**, 106003
- Song Y.-S., Percival W. J., 2009, *Journal of Cosmology and Astroparticle Physics*, 2009, 004–004
- Spergel D., et al., 2015, Wide-Field Infrared Survey Telescope–Astrophysics Focused Telescope Assets WFIRST-AFTA 2015 Report ([arXiv:1503.03757](https://arxiv.org/abs/1503.03757))
- Starobinsky A. A., 1980, *Phys. Lett. B*, **91**, 99
- Starobinsky A. A., 1983, *Sov. Astron. Lett.*, **9**, 302
- Steinhardt P. J., 2003, *Phil. Trans. Roy. Soc. Lond. A*, **361**, 2497
- Torrado J., Lewis A., 2021, *Journal of Cosmology and Astroparticle Physics*, 2021, 057
- Tsujikawa S., 2011, *Astrophysics and Space Science Library*, p. 331–402
- Tsujikawa S., 2013, *Classical and Quantum Gravity*, **30**, 214003
- Velten H. E. S., vom Marttens R. F., Zimdahl W., 2014, *The European Physical Journal C*, **74**
- Väliiviita J., Majerotto E., Maartens R., 2008, *Journal of Cosmology and Astroparticle Physics*, 2008, 020
- Whitt B., 1984, *Phys. Lett. B*, **145**, 176

This paper has been typeset from a $\text{\TeX}/\text{\LaTeX}$ file prepared by the author.